

Microfluidic Separation and Gateable Fraction Collection for Mass-Limited Samples

Joseph J. Tulock,^{†,‡} Mark A. Shannon,^{‡,§} Paul W. Bohn,^{*,†,‡} and Jonathan V. Sweedler^{*,†,‡}

Department of Chemistry, Department of Mechanical and Industrial Engineering, and Beckman Institute for Advanced Science and Technology, University of Illinois at Urbana–Champaign, 600 South Mathews Avenue, Urbana, Illinois 61801

Integrating multiple analytical processes into microfluidic devices is an important research area required for a variety of microchip-based analyses. A microfluidic system is described that achieves preparative separations by intelligent fraction collection of attomole quantities of sample. The device consists of a main microfluidic channel used to perform electrophoresis, which is interconnected at 90° to two vertically displaced channels via a nanocapillary array membrane. The membrane interconnect contains nanometer-diameter pores that provide fluidic communication between the channels. Sample injection and analyte collection are controlled by application of an electrical bias between the microfluidic channels across the nanocapillary array. After the separation, the automated transfer of the FITC-labeled Arg, Gln, and Gly bands occurs; a fluorescence detector located at the separation/collection channel interconnect is used to generate a triggering signal that initiates suitable voltages to allow near-quantitative transfer of analyte from the separation channel to the second fluidic layer. The ability to achieve such sample manipulations from mass-limited samples enables a variety of postseparation processing events.

The number and variety of analyses being adapted to microfluidic formats continues to grow, and the need to perform multiple-sample manipulations within a single device is a recurring theme for many applications. Examples of integrated microfluidic devices have been reported previously, with the earliest of these designed to perform precolumn or postcolumn reactions to enhance detection for separations.^{1–6} Recently a number of integrated devices for DNA analysis have been reported in which

restriction digestion, PCR amplification, separation and fractionation,⁷ and even cell lysis⁸ have been coupled.^{9–14} The challenges inherent in DNA characterization are similar to those encountered in proteomics, and integrated devices for protein analysis are likely to be important for the same reasons.¹⁵

The challenges associated with sequential manipulations required in both DNA and protein characterizations are exacerbated when the sample is mass-limited. Two types of samples naturally demand handling low-mass amounts: samples where the mass is limited by how much is available for characterization, and samples limited by some characteristic, e.g., toxicity or cost, of the analyte. Molecular messengers important in cellular signaling are an example of the first class, especially when cells are to be studied individually and population statistics built up from the single-cell level. Toxins illustrate the second class of mass-limited samples. For example, the highly potent microbially derived toxins from *Clostridium botulinum* are among the most potent neurotoxins known, with an LD₅₀ ~ 10⁻¹¹ g/kg,¹⁶ meaning that the lethal dose for a 50-kg individual is ~3 × 10⁻¹⁵ mol, clearly demanding that low sample masses be manipulated.

When mass-limited samples are encountered, it is often desirable to isolate components that produce a signal of interest, so that they can be amplified, modified, or coupled to conventional instrumentation, such as mass spectrometry, for identification. Such complex postprocessing schemes require that small-volume mass-limited samples first be fractionated after separation.¹⁷ Examples of microfluidic fraction collection in planar architectures, where fractions are collected in channels or reservoirs that are

* To whom correspondence should be addressed. E-mail: bohn@scs.uiuc.edu. sweedler@scs.uiuc.edu.

[†] Department of Chemistry.

[‡] Beckman Institute for Advanced Science and Technology.

[§] Department of Mechanical and Industrial Engineering.

- (1) Jacobson, S. C.; Hergenroder, R.; Moore, J.; Alvin, W.; Ramsey, J. M. *Anal. Chem.* **1994**, *66*, 4127–4132.
- (2) Fluri, K.; Fitzpatrick, G.; Chiem, N.; Harrison, D. J. *Anal. Chem.* **1996**, *68*, 4285–4290.
- (3) Harrison, D. J.; Fluri, K.; Chiem, N.; Tang, T.; Fan, Z. *Sens. Actuators, B* **1996**, *33*, 105–109.
- (4) Ro, W. K.; Lim, K.; Kim, H.; Hahn, J. H. *Electrophoresis* **2002**, *23*, 1129–1137.
- (5) Wang, J.; Chatrathi, M.; Tian, B. *Anal. Chem.* **2000**, *72*, 5774–5778.
- (6) Jacobson, S. C.; Koutny, L. B.; Hergenroder, R.; Moore, A. W.; Ramsey, J. M. *Anal. Chem.* **1994**, *66*, 3472–3476.

- (7) Khandurina, J.; Chovan, T.; Guttman, A. *Anal. Chem.* **2002**, *74*, 1737–1740.
- (8) Waters, L. C.; Jacobson, S. C.; Kroutchinina, N.; Khandurina, J.; Foote, R. S.; Ramsey, J. M. *Anal. Chem.* **1998**, *70*, 158–162.
- (9) Burns, M. A.; Mastrangelo, C. H.; Sammarco, T. S.; Man, F. P.; Webster, J. R.; Johnson, B. N.; Foerster, B.; Jones, D.; Fields, Y.; Kaiser, A. R.; Burke, D. T. *Proc. Natl. Acad. Sci. U.S.A.* **1996**, *93*, 5556–5561.
- (10) Woolley, A. T.; Hadley, D.; Landre, P.; deMello, A. J.; Mathies, R. A.; Northrup, M. A. *Anal. Chem.* **1996**, *68*, 4081–4086.
- (11) Jacobson, S. C.; Ramsey, J. M. *Anal. Chem.* **1996**, *68*, 720–723.
- (12) Burns, M. A.; Johnson, B. N.; Brahmasandra, S. N.; Handique, K.; Webster, J. R.; Krishnan, M.; Sammarco, T. S.; Man, P. M.; Jones, D.; Heldsinger, D.; Mastrangelo, C. H.; Burke, D. T. *Science* **1998**, *282*, 484–487.
- (13) Khandurina, J.; McKnight, T. E.; Jacobson, S. C.; Waters, L. C.; Foote, R. S.; Ramsey, J. M. *Anal. Chem.* **2000**, *72*, 2995–3000.
- (14) Hong, J. W.; Fujii, T.; Seki, M.; Yamamoto, T.; Endo, I. *Electrophoresis* **2001**, *22*, 328–333.
- (15) Bruin, G. J. M. *Electrophoresis* **2000**, *21*, 3931–3951.
- (16) Pellizzari, R.; Rossetto, O.; Schiavo, G.; Montecucco, C. *Philos. Trans. R. Soc. London B* **1999**, *354*, 259–268.
- (17) Ramsey, J. M., van Den Berg, A., Eds. *Micro Total Analysis Systems*; Kluwer Academic Publishers: Monterey, CA, 2001.

not fluidically isolated from the separation channels, have been reported.^{7,14,18,19} However, realizing the full potential of preparative separations on mass-limited samples will require the capacity to implement postprocessing reactions under solution conditions different from those used in the separation, requiring that the component of interest be physically isolated.

The work reported here focuses on developing hybrid nano-fluidic–microfluidic architectures that meet the demand for performing multidimensional chemical analysis, i.e., sequential sample manipulations, at low-mass levels. To address these issues, we developed and characterized devices that are capable of selectively transporting analytes, following their separation in a microfluidic electrophoresis channel, into a vertically displaced, fluidically isolated, collection channel.

Nanocapillary array membranes are employed to couple multiple, vertically separated microfluidic channels and to enable externally controllable fluidic communication between channels. To demonstrate the operational principles, sample injection, separation, and fractionation are performed within a single device on attomole quantities of fluorescein isothiocyanate (FITC)-labeled amino acids. These unit operations are completely automated, with switching between operating states controlled by monitoring the fluorescence of the analyte at the point of collection and using the presence of a fluorescence signal to trigger application of the appropriate voltage scheme to collect the sample. The work presented here represents a significant advance over our previous work in that, by automating multiple analytical operations within a single device, performing complex analysis such as multidimensional separations will be enabled. In this paper, we describe the operating modes, the critical control parameters, and the operational efficiencies achieved in this approach.

EXPERIMENTAL SECTION

Materials. Amino acids (>99%), FITC (>98%), and all buffer constituents were purchased from Aldrich Chemical Co. and used as received. Separation and collection experiments were performed using phosphate buffer solutions (5 mM; pH = 8.0) that were prepared in deionized water (Milli-Q; 18.2 M Ω cm). Poly-(dimethylsiloxane) (PDMS) was purchased from Dow Corning as a kit (Sylgard 184) containing prepolymer and initiator. Polycarbonate nanoporous membranes were purchased from Osmonics Inc. All membranes used in this work possessed 200-nm mean pore diameters.

FITC Derivatization of Amino Acids. Amino acids were derivatized with FITC in a manner similar to a previously described procedure.^{20,21} Stock solutions of individual amino acids were prepared in 10 mL of borate buffer (10 mM; pH = 9.0) by addition of the appropriate amount of each amino acid to produce final concentrations of 10 mM. Stock solutions were adjusted to a final pH = 9 by dropwise addition of 0.1 M NaOH, after which a 250- μ L aliquot of a 40 mM FITC stock solution in DMSO was added. The reaction of FITC with amino acids was allowed to proceed overnight in the dark with a 10:1 excess of the amino

acid with respect to FITC. For separation and collection experiments, solutions of FITC-labeled amino acids with the appropriate concentration were prepared by diluting aliquots of the borate buffer reaction solution with 10 mL of 5 mM phosphate buffer.

Device Fabrication. Microfluidic devices were fabricated according to established rapid prototyping protocols.^{22,23} Briefly, lithographic masters were fabricated by spin coating silicone wafers with the appropriate thickness of a negative photoresist (SU-850; MicroChem, Newton, MA). Lithographic masks were created as drawings in Adobe Illustrator and then printed as black and white transparencies on a commercially available high-resolution (5080 dpi) printer. Coated wafers were then covered with a lithographic mask and exposed to UV radiation (~450 mJ cm⁻² at 365 nm) thereby reproducing the desired features of the mask within the photoresist. Treatment of the exposed resist with developer solution removed any unexposed photoresist leaving raised features on the silicon wafer.

Fluidic channels (50 μ m \times 50 μ m cross section) were cast in PDMS by pouring a mixture of the prepolymer and initiator (10:1) over silicon masters and then curing the mixture at 110 $^{\circ}$ C for 1 h. Monoliths of cured PDMS containing channels were treated with an oxygen plasma (Texas Instruments RIE Module; 300 W, 500 mTorr, 20 s) making the complementary PDMS surfaces reactive to one another. The treated surfaces were then joined with their channels facing one another, and the assembled device was heated in a temperature-controlled oven at 110 $^{\circ}$ C for at least 3 h. Nanofluidic interconnects were formed by placing rectangular pieces (2 mm \times 5 mm) of PCTE membranes at the intersection of the crossed microfluidic channels before joining the plasma-treated monoliths of PDMS.^{24,25}

Instrumentation. Separation and collection experiments were performed using a dual-beam laser-induced fluorescence (LIF) detection system fabricated from discrete components (Figure 1). The output (488 nm) from an Ar⁺ ion laser (Melles Griot 532 series) was directed onto a beam splitter (50/50 at 488 nm) which, along with flat mirrors, directed each beam (~7 μ W) to separate sets of epifluorescence optics. Microscope objectives (10 \times) positioned above and below the electrophoresis channel were used to focus the incident beams within PDMS devices and to collect fluorescence emission from FITC-labeled amino acids. For separation and collection experiments, the first detection point was located at the collection gate and served as a triggering signal to activate the devices into the collection state. The second detection point was placed downstream of the collection gate and was used to monitor separations performed with and without collection of analytes. Fluorescence emission was detected with photon counting PMT modules (Hamamatsu, model HC124), which were mounted in a light-tight housing of Delrin coupled with a 150- μ m pinhole, long-pass emission filter (Melles Griot, GG 495) and mechanical shutter (Uniblitz). Sample injection, separation, and collection were controlled remotely via application of electrical potentials to Pt electrodes placed in on-chip fluidic reservoirs. The

(18) Ramond, D. E.; Manz, A.; Widmer, H. M. *Anal. Chem.* **1996**, *68*, 2515–2522.

(19) Ramond, D. E.; Manz, A.; Widmer, H. M. *Anal. Chem.* **1994**, *66*, 2858–2865.

(20) Moore, A. W.; Jorgenson, J. W. *Anal. Chem.* **1993**, *65*, 3550–3560.

(21) Van Den Beld, C. M. B.; Lingeman, H.; Van Ringen, G. J.; Tjaden, U. R.; Van Der Greef, J. *Anal. Chim. Acta* **1988**, *205*, 15–27.

(22) Duffy, D. C.; McDonald, J. C.; Schueller, J. A.; Whitesides, G. M. *Anal. Chem.* **1998**, *70*, 4974–4984.

(23) Jo, B.-H.; Van Lerberghe, L. M.; Motsegood, K. M.; Beebe, D. J. *J. Microelectromech. Sys.* **2000**, *9*, 76–81.

(24) Cannon, D. M., Jr.; Kuo, T.-C.; Bohn, P. W.; Sweedler, J. V. *Anal. Chem.* **2003**, *75*, 2224–2230.

(25) Kuo, T.-C.; Cannon, D. M., Jr.; Chen, Y.; Tulock, J. J.; Shannon, M. A.; Sweedler, J. V.; Bohn, P. W. *Anal. Chem.* **2003**, *75*, 1861–1867.

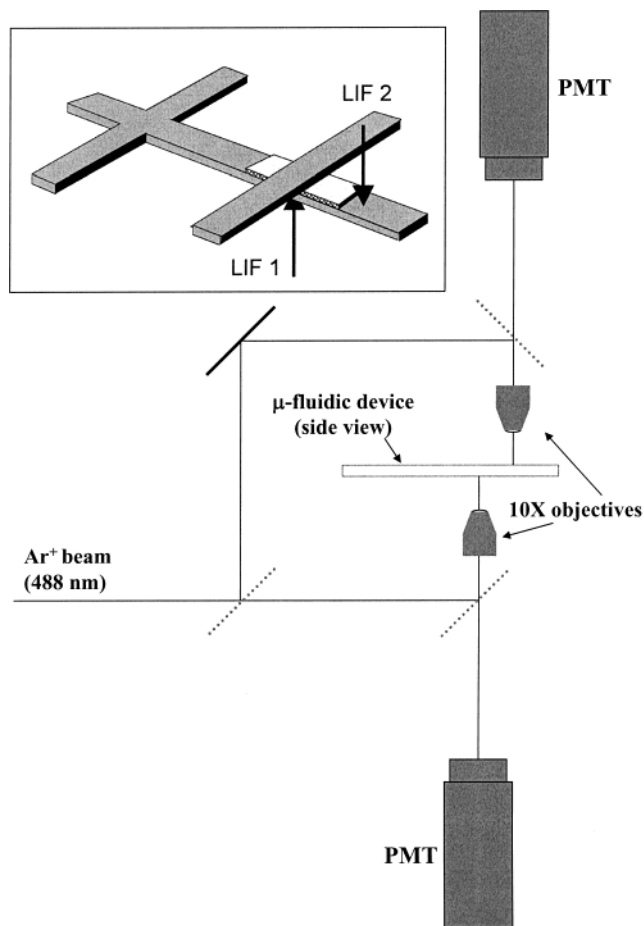


Figure 1. Schematic representation of the dual-beam LIF detection system used to perform separation and fractionation experiments. Dichroic beam splitters are represented by dashed lines; a 50/50 beam splitter is represented by a solid gray line, with a single flat mirror represented as a solid black line. (Inset) Schematic perspective view of the hybrid device. Electrophoresis occurs in the long channel, and the nanocapillary array membrane is depicted by the lightly shaded region where the CE channel crosses the collection channel. The positions of the detection laser-induced fluorescence measurements are denoted LIF1 and LIF2, respectively.

voltage supplies, an eight-switch voltage relay controller, shutter controllers, and signal acquisition were computer-controlled using National Instruments data acquisition cards and custom Labview software.

RESULTS AND DISCUSSION

Zero Cross Detection for Peak Recognition. The strategy for peak identification and collection is dictated by the spatial arrangement of LIF detection locations relative to the sample collection membrane, as shown in Figure 1. Briefly, the presence of a peak is detected by the LIF1 signal recorded at the collection interconnect, and if it is the desired peak (identified by peak number), the fluid transport voltages are switched to allow the collection of that peak alone based on the measured peak parameters such as peak amplitude determined in real time. The inset shows a perspective view of the electrophoresis and collection channels relative to the position of the LIF measurement points.

To identify peaks arriving at the collection gate, the fluorescence signal LIF1 is collected directly at the collection membrane,

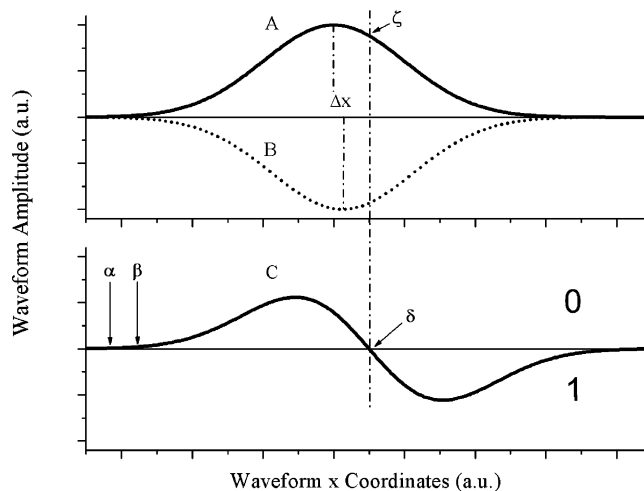


Figure 2. Schematic illustration of the detection of an idealized band from an electropherogram using the zero cross algorithm (A). Detection of the zero crossings (C) is achieved by subtracting the real-time value of (A) from that value of (A) which precedes it by Δx (represented by trace B). Using this algorithm, the traces must exhibit a crossing of the x -axis (δ) on the trailing edge (ζ) of the original signal (A). The high-frequency zero crossings associated with noise (α and β) are rejected by establishing a frequency cutoff above an established threshold.

and a peak count signal is calculated in real time. Collecting information about sample content directly at the nanocapillary array membrane obviates the need for a programmed delay between peak identification and initiation of peak collection.²⁶ In this way, peaks are collected by programming the computer to turn the collection state on immediately when a peak of interest is identified, since this also corresponds to the arrival of peaks at the collection gate. The challenges, then, are to (1) identify peaks against background noise, while preventing the occurrence of false positives/negatives, (2) transmit this information to the decision/control circuitry, and (3) transfer the band of interest with high efficiency.

Numerous peak picking algorithms exist, with varying levels of complexity depending on the need to perform baseline correction for quantifying peak areas.^{27–29} However, the automated peak collection experiments only require that the presence or absence of analyte bands be recognized. A simple and convenient approach to achieve this is shown in Figure 2, which illustrates the process of converting the fluorescence output to a zero cross format (C) of an idealized signal (A). If the peaks occurring in the electropherogram are approximately Gaussian, standard zero cross detection can be performed by subtracting the original signal (A) from itself, offset (B) by Δx . The offset, Δx , is defined with respect to a contiguous set of data points on the signal, $f(x)$, such that every point of the new function $g(f(x))$ is generated as

$$g(f(x)) = f(x_n) - f(x_{n-z}) \quad (1)$$

where x_n is the real-time value of the signal and x_{n-z} is the recorded

(26) Minarik, M.; Foret, F.; Karger, B. L. *Electrophoresis* **2000**, *21*, 247–254.

(27) Lee, Y. H.; Kassam, S. A. *IEEE Trans. ASSP* **1985**, *33*, 672.

(28) Rabiner, L. R.; Sambur, M. R.; Schmidt, C. E. *IEEE Trans. ASSP* **1975**, *23*, 552.

(29) Gallagher, N. C.; Wise, G. L. *IEEE Trans. ASSP* **1982**, *29*, 1136.

value of the signal preceding x_n by z data points.³⁰ Every point, p , on the resulting trace is assigned a value of 0, where $g(f(x)) \geq 0$, and 1, where $g(f(x)) < 0$. A running total of these values is kept and zero crossings are identified as a change in this running total. To reject noise, zero crossings occurring within less than 11 sampling cycles (10-Hz sampling frequency) from each other are rejected. This rejection criterion was experimentally determined to efficiently reject noise, while correctly identifying peaks. As shown in Figure 2, the trace resulting from an electropherogram peak exhibits a zero crossing that occurs at the trailing edge of the signal waveform (ζ). The initial tuning of Δx , signal sampling rate, and frequency rejection criteria can be performed in less than a half of a day of experimentation. However, once these values are determined, little or no further tuning is required.

For the purposes of capturing bands, triggering the gate on the trailing edge of a peak is as effective as triggering at the peak maximum. It is easy to implement, resistant to noise, and allows bands to be effectively captured (vide infra). The autocorrelation method is similar to "slope threshold" methods³¹ used for peak picking; however, noise rejection is achieved by applying a frequency rejection criterion for zero crossings, instead of signal smoothing strategies. To reduce the possibility of false positives, zero crossing not associated with a signal level above an established detection limit ($s + 5\sigma$) can be rejected, the detection limit being determined by statistical analysis of an assigned range of baseline data at the beginning of each experiment.

The effectiveness of the zero cross method of peak detection was evaluated by performing separations of a mixture of FITC-labeled amino acids—Arg, Gln, Gly, and Ser. Figure 3 shows the electropherograms, along with the calculated peak detection traces for three repeated separations of the FITC-labeled amino acids. The noise rejection of the peak recognition algorithm is evident in the lack of false peak identifications. Despite numerous occurrences of zero crossings associated with noise, only those zero crossings associated with an analyte are recognized as true peaks. In addition, while the peaks associated with Gln, Gly, and Ser are not completely resolved, they are still recognized as individual peaks. This was not true of the doublet of peaks exhibited by Arg, because the zero crossings produced by this set of peaks are spaced closely enough that the second crossing is rejected by the detection algorithm. However, if it were necessary to recognize the individual components of this doublet as separate bands, they could readily be identified as such by adjusting the signal sampling rate and peak detection criteria. As expected, the separated bands are recognized on the trailing edge.

Microchip Operation. The nanocapillary array membrane, which establishes switchable fluidic communication between the vertically separated microfluidic channels, is pivotal in establishing the ability to fractionate individual components into independent collection channels.^{24,25,32} Figure 4 shows a photograph of a hybrid nanofluidic-microfluidic device containing two such interconnects: one (left) which serves as a sample injection gate for the main electrophoresis channel,²⁴ and another (right) which serves

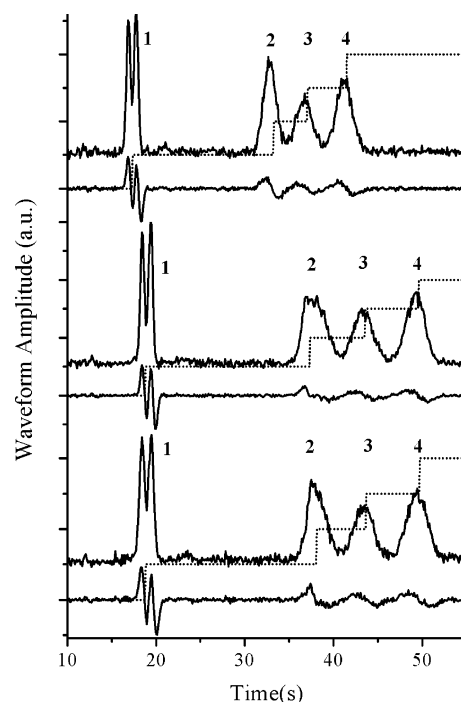


Figure 3. Three repetitive trials of the peak detection algorithm for real-time band recognition during the separation of the FITC-labeled amino acids Arg, Gln, Ser, and Gly ($1 \mu\text{M}$ each). In each separation, the electropherogram recorded at the collection gate is shown immediately above the corresponding trace (offset for clarity). The dotted traces represent the computer-generated peak count as determined from the collection gate triggering signal. Separations use 5 mM phosphate buffer (pH = 8) with $E = 625 \text{ V/cm}$.

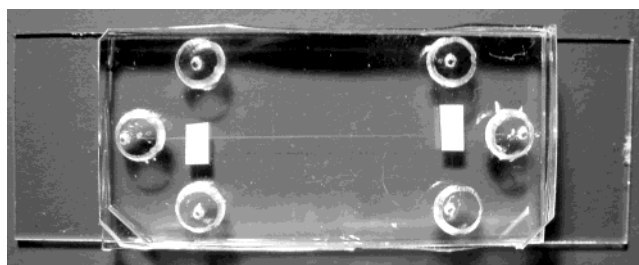


Figure 4. Photograph showing a top view of a typical microfluidic device used to perform separation and sample fractionation experiments. The device contains two nanoporous membranes (white rectangles), which couple a sample injection channel (left) and a peak collection channel (right) to the separation channel (horizontal).

to capture targeted analytes. Using an independent nanocapillary array as an injection gate simplifies the voltage schemes needed to achieve injections.^{1,33–40}

(30) O'Conner, D. V.; Phillips, D. *Time-correlated single photon counting*, Academic Press: London, 1984.

(31) *Handbook of Capillary Electrophoresis*, 2nd ed.; CRC Press: Boca Raton, FL, 1997.

(32) Kuo, T.-C.; Cannon, D. M.; Shannon, M. A.; Bohn, P. W.; Sweedler, J. V. *Sens. Actuators, A* **2003**, *A102*, 223–233.

(33) Effenhauser, C. S.; Manz, A.; Widmer, H. M. *Anal. Chem.* **1993**, *65*, 2637–2642.

(34) Jacobson, S. C.; Hergenroder, R.; Koutny, L. B.; Warmack, R. J.; Ramsey, J. M. *Anal. Chem.* **1994**, *66*, 1107–1113.

(35) Koutny, L. B.; Scmalzing, D.; Taylor, T. A.; Fuchs, M. *Anal. Chem.* **1996**, *68*, 18–22.

(36) Harrison, D. J.; Manz, A.; Fan, Z.; Ludi, H.; Widmer, H. M. *Anal. Chem.* **1992**, *64*.

(37) Effenhauser, C. S. *Anal. Methods Instrum.* **1993**, *1*, 172–176.

(38) Fu, L.-M.; Yang, R.-J.; Lee, G.-B.; Pan, Y.-J. *Electrophoresis* **2003**, *24*, 3026–3032.

(39) Arlaire, J. P.; Jacobson, S. C.; Ramsey, J. M. *Electrophoresis* **2001**, *22*, 312–317.

(40) Arlaire, J. P.; Jacobson, S. C.; Culbertson, C. T.; Ramsey, J. M. *Electrophoresis* **2000**, *21*, 100–106.

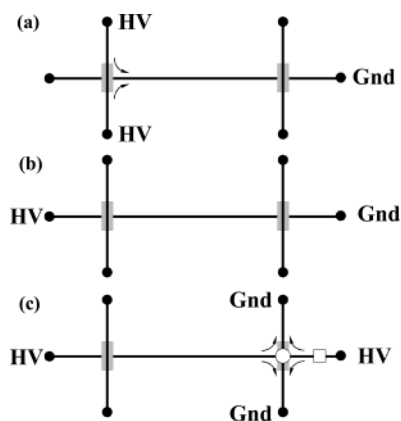


Figure 5. Schematic diagram showing the configuration of voltages applied to the fluid reservoirs in order to achieve (a) sample injection, (b) separation, and (c) band collection. Fluid flow directions during injection and collection are shown by the arrows near the nanocapillary array membrane. Reservoirs not labeled are allowed to float. The locations of the collection LIF (circle), and postgate detection LIF (square) detection zones used for all experiments are indicated in (c). The detection zones, not shown to scale, are separated by 5 mm. The pre- and postgate channel segments are 39 and 9 mm, respectively.

The voltages used for injection and separation are shown in Figure 5. In each case, fluid motion is driven by voltages applied to Pt wire electrodes placed in the fluidic reservoirs. When sample transfer across a nanocapillary array membrane is required to inject a sample plug, high voltage is applied to each sample channel reservoir while holding the waste reservoir of the electrophoresis channel at ground. A slightly more complex voltage scheme is used for preparative band collection. Collections can be performed with a voltage configuration similar to that used for injection, raising the applied voltage of the buffer reservoir of the electrophoresis channel while holding the collection channel at ground. However, this configuration induces fluid to flow through the gate region only from the pregate section of the electrophoresis channel. The peak widths are typically $\sim 1\text{--}3$ mm wide, while the collection gate region is $50\ \mu\text{m}$ wide. Thus, if the postgate portion of the electrophoresis channel is not routed through the collection gate, some portion of the bands of interest is not collected. The collection voltage scheme shown in Figure 5c maximizes peak collection by reversing fluid flow in the postgate section from the waste reservoir toward the collection gate. Thus, the collection bias scheme is designed so that fluid approaching the nanocapillary array membrane from either direction in the electrophoresis channel is transported from the separation channel to the collection channel through the nanocapillary array, subsequently flowing away from the nanocapillary array in both directions in the collection channel.

It is important to consider the volume flow rates in the pre- and postcollection gate segments of the electrophoresis channel, since they directly influence the efficiency of the collection process. When the signal monitored at the collection gate, LIF1 in Figure 1, falls below an established threshold, the collection process is halted. If different fluid flow rates are present on opposite sides of the collection gate, it is possible for band pileup to occur, where a portion of the targeted band remains in the detection volume, while additional peaks migrate into the collection zone before complete collection of the targeted peak. This

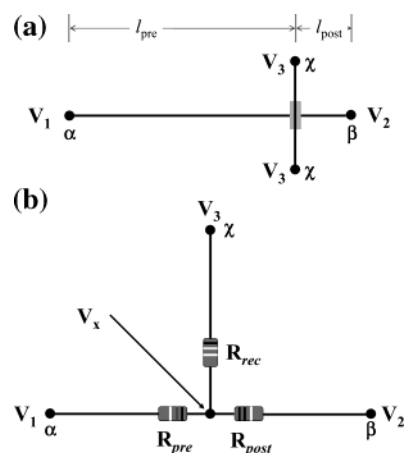


Figure 6. (a) Schematic diagram showing the generic voltages and segment lengths relevant to the collection state. The voltages applied at the buffer, buffer waste, and collection gate reservoirs are V_1 , V_2 , and V_3 , respectively. V_1 and V_2 are controlled by separate voltage supplies, while both reservoirs of the collection channel are biased by a common voltage source. The injection channel and its associated nanocapillary membrane are omitted for clarity. (b) Equivalent circuit diagram of the device in its collection state. R_{pre} and R_{post} represent the resistance of the pre- and postgate channel segments. R_{rec} represents the resistance of the nanocapillary array membrane combined in series with the resistance of the microfluidic collection channel.

problem can be minimized by establishing equal volume flow rates in the pre- and postgate segments of the electrophoresis channel.

To control fluid flow in these channel segments, it is necessary to control the electric field strength in each segment during the collection process, as the volume flow in each channel is proportional to field strength.⁴¹ The field strength present in each channel is

$$E = \Delta V/l \quad (2)$$

where ΔV is the voltage drop across a channel segment of length l . The voltages V_1 , V_2 , and V_3 necessary to produce equal field strengths in channel segments l_{pre} and l_{post} can be calculated by modeling the device as a network of impedances as shown in Figure 6. According to Kirchoff's law of current, the voltage drop experienced by each channel segment is related to its resistance according to

$$\frac{V_x - V_3}{R_{\text{rec}}} = \frac{V_1 - V_x}{R_{\text{pre}}} + \frac{V_2 - V_x}{R_{\text{post}}} \quad (3)$$

where V_x is the potential in the electrophoresis channel at the interconnect and R_{pre} (162 M Ω), R_{post} (32 M Ω), and R_{rec} (20 M Ω) are the resistances of the pregate, postgate, and receiving channel segments, respectively, where the numerical values refer to the specific device used to produce the data in Figure 2. R_{pre} , R_{post} , and R_{rec} were determined by measuring the resistance of the electrical pathways formed between points (α, χ) , (α, β) , and (β, χ) (Figure 6b). The resistances $R(\alpha\chi)$, $R(\alpha\beta)$, and $R(\beta\chi)$ represent

(41) Weinberger *Practical Capillary Electrophoresis*, 2nd ed.; Academic Press: San Diego, CA, 2000.

Table 1. Device Parameters Determining Electrokinetic Flow during Separation and Collection

	V_1 (V) ^a	V_2 (V) ^a	V_3 (V) ^a	E (V/cm)	
				pre	post
separation	3000	0	float	625	625
collection	562	222	0	113	113

^a Voltage designations are referenced to the positions in Figure 6.

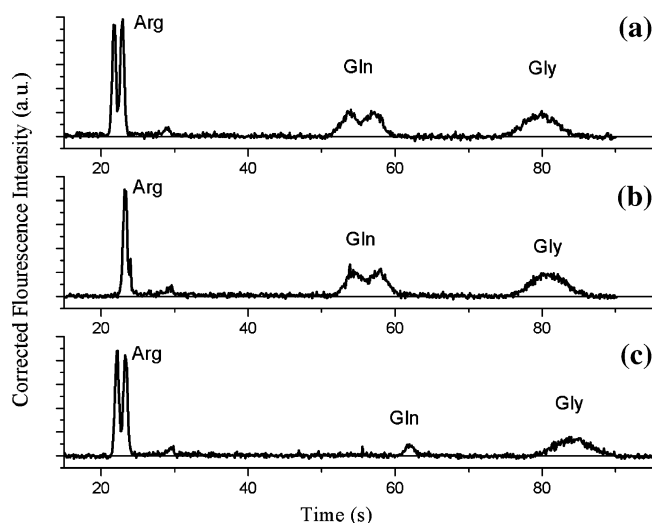


Figure 7. Electropherograms of FITC-labeled Arg, Gln, and Gly: (a) no collection; (b) collection of the first component of the Arg doublet peak; (c) collection of the Gln band. Separation conditions: 5 mM phosphate buffer (pH = 8) at a field strength of 625 V/cm.

linear combinations of the resistances, R_{pre} , R_{post} , and R_{rec} , which can be calculated via simultaneous algebraic equations relating $R(\alpha\gamma)$, $R(\alpha\beta)$, and $R(\beta\gamma)$. According to eq 2, the field strengths in segments I_{pre} and I_{post} are equal if $(V_1 - V_2) = 4.33 (V_2 - V_3)$. By substituting this relationship into eq 3 and assuming the receiving channel is at ground ($V_{rec} = 0$), the necessary voltages are calculated for any value of V_{pre} . Table 1 summarizes the voltages defining the separation and collection states for one particular operational state.

Separation and Collection. Separation and sample fractionation experiments were performed on a mixture of FITC-labeled Arg, Gln, and Gly, as illustrated in Figure 7. The electropherograms shown are those recorded at the postgate detector and demonstrate the feasibility of automating microchip-based separations and sample fractionation on mass-limited samples. The electropherogram in Figure 7a shows the separation of the FITC-labeled amino acids with no collection. The Arg, Gln, and Gly peaks are well resolved with Arg and Gln appearing as doublets, because they each possess two primary amines, and reaction with FITC at both locations produces two labeled products. We also note that the peaks as detected at the postgate detector exhibit Gaussian shape and have not been distorted by the presence of the nanocapillary interconnect. We also do not observe anomalous increases in peak widths between detection of peaks before and after the interconnect. The electropherograms in Figure 7b and c were recorded with collection of the Arg and Gln bands, respectively. Band collection was performed by enabling the

collection feature of the software and entering the anticipated peak number of the target peak as determined from prior separation experiments. During collection experiments, no user input is needed to initiate collection or to resume separation once the target peak has been collected. Switching between the separation and collection voltages is automated by the signal monitored at the collection gate. Figure 7b shows the result of a collection experiment where the first Arg band was targeted for collection. Nearly complete collection of the first Arg component is evidenced by the appearance of this band as a single peak with a slight shoulder, in contrast to the doublet exhibited by Arg when no collection is performed. Also, the uncollected Arg band and the Gln and Gly bands appear at slightly longer migration times than in the noncollected electropherogram in Figure 7a. The delay in migration times arises because the field strength within the separation channel is lower during collection than during separation; cf. Table 1. Similar results were observed when both components of the Gln band were targeted for collection, as shown in Figure 7c. A small portion of the Gln bands remains after collection and reaches the detection zone at ~60 s, again slightly delayed from the migration time observed for Gln when no collection was performed. The Gly band also exhibits a slightly longer migration time, as expected. However, in Figure 7c, the Arg doublet exhibits the same migration time as in the noncollected electropherogram, because Arg passes the detection point and enters the buffer waste reservoir before collection of Gln is initiated.

It is interesting to contrast the efficiency of the automated collection of Arg and Gln with each other and with manually collected bands using similar nanocapillary array membranes.²⁵ The capture efficiency of each peak can be calculated by calculating the ratio of peak areas (Arg/Gln/Gly) when both separation and collection are performed to the peak areas when only a separation is performed. This yields 43% collection efficiency for Arg, while Gln is collected with 86% efficiency. This analysis ignores the fact that the Arg band is composed of a sharp doublet and that the first component of the doublet is collected with near-quantitative efficiency. The difference between the Arg and Gln collection efficiency highlights the interaction of the peak detection approach with the control algorithm used to implement the collection bias scheme. Under the conditions used in Figure 7b and c, the Arg doublet is better resolved than the bands associated with Gln. The signal, thus, is more likely to decrease to its threshold value during collection as the resolution between the two bands of a doublet increases. The electrophoretic mobilities of Arg and Gly may also play a role in determining the transport behavior of these analytes across the nanofluidic interconnect and may influence the behavior of signals recorded during collection.

The fact that neither peak is completely collected is expected. The collection process has been programmed to stop when the signal decreases to a preset threshold value, corresponding to a signal level where a portion of peaks must remain in the separation channel. Higher collection efficiencies can be realized if the collection process is programmed to stop when the zero cross detection signal from LIF1 decreases to baseline, which would also decrease the effective resolution of the collected component. These automated collections can also be compared to the manual nanocapillary array-mediated sample collection reported previ-

ously, *viz.* Figure 9 of ref 25, where Arg and Glu were separated and sampled. In the manual implementation, collection was performed at the detection limit of our laser-induced fluorescence detection scheme (i.e., 100% of the desired bands). This was accomplished by repeating the separation several times, calculating the projected arrival time of the leading edge of the desired band and its temporal width, and then forward biasing the collection gate during the appropriate time window containing the band of interest. It is possible to combine the features of both approaches—using the zero crossing control algorithms described here with LIF detector preceding the point of collection. By implementing the peak detection strategy at a detection location preceding the collection point, the widths of peaks could be extracted from the information contained in both the raw signal and zero cross function. In this way, tailoring the duration of the collection pulse could be automated and used as an additional control parameter, along with signal monitored at the collection point, to achieve the highest degree of flexibility and performance.

It is also important to consider how much material is being collected. Fluorescence micrographs indicate that, for an injection duration of 0.2 s, the sample spans $\sim 50 \mu\text{m}$ of channel length, corresponding to a plug volume of 120 pL. Although the concentration of sample is expected to decrease after injection,³² an analyte concentration of 1×10^{-6} M following injection corresponds to 1.2×10^{-16} mol (120 amol) of each amino acid. Since the detection system is obviously capable of working with orders of magnitude lower concentrations, these results establish the ability to collect and manipulate small-volume mass-limited samples.

To summarize, the preparative sampling of attomole quantities of labeled amino acids within a hybrid nanofluidic/microfluidic

device has been studied. The work demonstrates the capability to do the following: (1) sense the presence of analyte bands in the electrophoresis channel based on a LIF signal recorded at the point of collection; (2) use the LIF signal to trigger transfer of individual analyte bands into a receiving channel physically isolated from the separation channel; and (3) resume the separation to remove the slower moving bands from the separation channel. The ability to capture analyte bands selectively is an important step toward enabling complex postseparation processing of analytes, because bands of interest can now be sequestered in fluidically isolated channels. These processes are enhanced by exploiting the nanocapillary array membranes to collect analytes from one fluidic environment and move it into a separate fluidic environment, with each containing ionic strength, pH, or composition optimized for particular analytical tasks—as examples, multi-dimensional separations using differing electrolyte conditions or independently optimized separation and detection buffers.

ACKNOWLEDGMENT

This work was supported by the NanoCEMMS Center sponsored by the National Science Foundation under Grant DMI-0329162, by the Defense Advanced Research Projects Agency under Grant F30602-00-2-0567, and by the National Institute of Allergies and Infectious Diseases through Grant U54 AI57153-01, which supports the Great Lakes Regional Center for Excellence.

Received for review March 15, 2004. Accepted August 11, 2004.

AC049601P